

Image fusion with additive multiresolution wavelet decomposition.

Applications to SPOT+Landsat images

Jorge Núñez, Xavier Otazu, and Octavi Fors

Departament d'Astronomia i Meteorologia, Universitat de Barcelona, E-08028 Barcelona, and Observatori Fabra, Barcelona, Spain

Albert Prades

Escola Universitaria Politècnica de Barcelona, Universitat Politècnica de Catalunya, E-08028, Barcelona, Spain

Vicenç Palà and Román Arbiol

Institut Cartogràfic de Catalunya, Parc de Montjuïc, E-08038 Barcelona, Spain

Received February 27, 1998; accepted September 29, 1998; revised manuscript received October 16, 1998

A technique based on multiresolution wavelet decomposition was developed for the merging and data fusion of a high-resolution panchromatic image and a low-resolution multispectral image. The standard data fusion methods may not be satisfactory, because they can distort the spectral characteristics of the multispectral data. The method presented here consists of adding the wavelet coefficients of the high-resolution image to the multispectral (low-resolution) data. More specifically, we add the high-order coefficients of the wavelet transform of the panchromatic image to the intensity component (L) of the multispectral image. The method is thus an improvement on standard intensity-hue-saturation (IHS or LHS) mergers. An alternative approach for correcting the red-green-blue coefficients is also discussed. We used the method to merge SPOT and Landsat Thematic Mapper images (SPOT means *Système pour l'Observation de la Terre*). The technique presented is clearly better than the IHS and LHS mergers for preserving both spectral and spatial information. © 1999 Optical Society of America [S0740-3232(99)00403-2]

OCIS codes: 100.7410, 100.0100, 100.2980, 280.0280.

1. INTRODUCTION

There are several situations that require high spatial and high spectral resolution simultaneously in a single image. This is particularly important in remote sensing. In other cases, for example, in astronomy, high spatial resolution and high signal-to-noise ratio may be required. However, in most cases instruments are not capable of providing such data, either because of design or because of observational constraints. For example, in remote sensing, SPOT-PAN satellite data provide high-resolution (10-m pixels) panchromatic data (SPOT means *Système pour l'Observation de la Terre*; PAN means panchromatic), whereas Landsat Thematic Mapper (TM) satellite data provide lower-resolution (30-m pixels) multispectral images. In astronomy, space-borne telescopes give high-resolution images, but the photons are expensive to collect, thus making long-exposure multispectral observations unusual. From the ground, however, the resolution is poor, but the photons are cheap to collect and the signal-to-noise ratio can be increased. In addition, it is easy to obtain long-exposure (but low-resolution) multispectral data from the ground.

One possible solution comes from the field of data fusion.¹ A number of methods have been proposed for merging panchromatic and multispectral data.^{2,3} The

most common procedures are methods based on intensity-hue-saturation transform (IHS and LHS mergers).^{4,5} However, the IHS and LHS methods produce spectral degradation. This is particularly crucial in remote sensing if the images to merge were not taken at the same time. In the past few years multiresolution analysis has become one of the most promising methods for the analysis of images in remote sensing.⁶ Recently, several authors (Yocky,^{7,8} Garguet-Duport *et al.*,⁹ Ranchin *et al.*¹⁰) proposed a new approach to image merging that uses a multiresolution analysis procedure based on the discrete two-dimensional wavelet transform. Núñez *et al.*¹¹ also carried out a preliminary study of the wavelet-based method in combination with image reconstruction. The wavelet approach preserves the spectral characteristics of the multispectral image better than the standard IHS or LHS methods.

Wavelet-based image merging can be performed in two ways: (i) by replacing some wavelet coefficients of the multispectral image with the corresponding coefficients of the high-resolution image and (ii) by adding high-resolution coefficients to the multispectral data. Here we further explore the wavelet transform image merging technique with special attention given to the additive merger. To decompose the data into wavelet coefficients,

we use the discrete wavelet transform algorithm known as *à trous* (with holes). The method is applied to merge SPOT and Landsat (TM) images.

2. STANDARD MERGING METHODS

The standard merging methods are based on the transformation of the red–green–blue (RGB) multispectral channels into the intensity–hue–saturation components.¹² Intensity refers to the total color brightness, hue refers to the dominant or average wavelength that contributes to a color, and saturation refers to the purity of a color relative to gray. With the standard methods the usual steps to perform are the following:

1. Register the low-resolution multispectral image to the same size as the high-resolution panchromatic image so that it is superimposed.
2. Transform the R, G, and B bands of the multispectral image into the intensity–hue–saturation components.
3. Modify the high-resolution panchromatic image to take into account the spectral differences with respect to the multispectral image, the different atmospheric and illumination conditions, etc. This is usually performed by conventional histogram matching between the panchromatic image and the intensity component of the intensity–hue–saturation representation. Specifically, after computation of the histogram of both the panchromatic image and the intensity component of the multispectral image, the histogram of the intensity (of the multispectral image) is used as a reference to which we match the histogram of the panchromatic image.
4. Replace the intensity component with the panchromatic image, and perform the inverse transformation to obtain the merged RGB image with merged panchromatic information.

Throughout this paper we assume that all RGB values are scaled over the 0–255 range.

The result of the standard merging methods depends on the intensity–hue–saturation system used. Many intensity–hue–saturation transformation algorithms have been developed for converting RGB values. Although the complexity of the models varies, the algorithms produce similar values for hue and saturation. However, the algorithms differ in the method used for calculating the intensity component of the transformation. The most common intensity definitions are

$$\begin{aligned}
 I &= I(R, G, B) = \max(R, G, B), \\
 L &= L(R, G, B) = (R + G + B)/3, \\
 L' &= L'(R, G, B) = [\max(R, G, B) \\
 &\quad + \min(R, G, B)]/2.
 \end{aligned}$$

We call the systems based on these definitions IHS, LHS, and L'HS color systems, respectively. The first system (based on I), also known as Smith's hexcone,¹² ignores two of the components to compute the intensity and will produce equal intensity for a pure color, e.g., $I = I(255, 0, 0) = 255$ and for a white pixel $I = I(255, 255, 255) = 255$. However, the second system (based on

L), known as Smith's triangle model,¹² would produce intensities of $L = L(255, 255, 255) = 255$ for a white pixel but only $L = L(255, 0, 0) = 85$ for a pure color. The third system (based on L')¹³ would again produce a result of $L' = L'(255, 255, 255) = 255$ for the white pixel and $L' = L'(255, 0, 0) = 125$ for a pure color.

Furthermore, the transformation algorithm based on the third definition (L') shows bizarre behavior in some cases. For example, if we have RGB values of $(R, G, B) = (100, 150, 200)$, transform them to the L'HS system, thus obtaining $(L'HS) = (150, 210, 0.476)$, add 10 counts (over a maximum of 255) to the L' component (now $L' = 160$), and reverse the transformation [$R = R(160, 210, 0.476) = 115$, $G = G(160, 210, 0.476) = 160$, $B = B(160, 210, 0.476) = 205$]; the resulting RGB values are $(R, G, B) = (115, 160, 205)$; i.e., the color with the lowest value (R) is the one that has the largest increment, whereas the component with highest value (B) has the lowest increment. However, if we transform the same RGB values $(R, G, B) = (100, 150, 200)$ to the LHS system, thus obtaining $(LHS) = (150, 210, 0.333)$, and again add 10 counts to the L component (now $L = 160$) and reverse the transformation, the RGB values would be $(R, G, B) = (107, 160, 213)$. In this case the increment of ten counts in the intensity is distributed proportionally to the values of the R, G, and B components.

Thus in this paper we prefer the definition $L = (R + G + B)/3$ for the intensity component, although we use both IHS- and LHS-based standard merging methods to compare our results. When this component is defined as $L = (R + G + B)/3$ it is also called lightness.

3. WAVELET DECOMPOSITION

Multiresolution analysis based on the wavelet theory permits the introduction of the concepts of details between successive levels of scale or resolution.^{14–19}

Wavelet decomposition is being used increasingly for the processing of images.^{20,21} The method is based on the decomposition of the image into multiple channels on the basis of their local frequency content. The wavelet transform provides a framework for decomposing images into a number of new images, each with a different degree of resolution. The wavelet representation is an intermediate representation between the Fourier and the spatial representation. In the Fourier transform we know the global frequency content of our image, but we have no information about the spatial localization of these frequencies. However, the wavelet transform gives us an idea of both the local frequency content and the spatial distribution of these frequencies. Since in Fourier space the base functions are sinusoidal, they extend along all space and do not have spatial concentration. But wavelets are concentrated around a central point; thus they have a high degree of spatial localization.

A. Theory

Below, we present the basics of the wavelet transform, relying on the multiresolution signal representation concept.^{6,22} First, we present one-dimensional formulas that can be extended easily to the two-dimensional case.

Given a signal $\mathbf{f}(t)$, we construct a sequence $\mathbf{F}_m[\mathbf{f}(t)]$ of approximations of $\mathbf{f}(t)$. Each $F_m[\mathbf{f}(t)]$ is specific for the representation of the signal at a given scale (resolution). $F_m[\mathbf{f}(t)]$ represents the projection of the signal $\mathbf{f}(t)$ from the signal space \mathbf{S} onto subspace \mathbf{S}_m . In this representation $F_m[\mathbf{f}(t)]$ is the closest approximation of $\mathbf{f}(t)$ with resolution 2^m .

The differences between two consecutive scales $m + 1$ and m are the multiresolution wavelet planes or detail signal at resolution 2^m :

$$w_m[\mathbf{f}(t)] = F_{m+1}[\mathbf{f}(t)] - F_m[\mathbf{f}(t)]. \quad (1)$$

This detail signal can be expressed as

$$w_m[\mathbf{f}(t)] = \sum_n W_{m,n}(\mathbf{f})\psi_{m,n}(t), \quad (2)$$

where coefficients $W_{m,n}(\mathbf{f})$ are given by the direct wavelet transform of the signal $\mathbf{f}(t)$:

$$W_{m,n}(\mathbf{f}) = \int_{-\infty}^{+\infty} \mathbf{f}(t)\psi_{m,n}(t)dt. \quad (3)$$

In the direct wavelet transform (3), m and n are scaling and translational parameters, respectively. The coefficients $W_{m,n}(\mathbf{f})$ are called wavelet coefficients of $\mathbf{f}(t)$. Such coefficients correspond to the fluctuations of the signal $\mathbf{f}(t)$ near the point n at resolution level m . Thus the wavelet transform (3) represents the expansion of signal $\mathbf{f}(t)$ in the set of basis functions $\psi_{m,n}(t)$. These basis functions are scaled and translated versions of a general function $\psi(t)$ called mother wavelet. To construct the basis functions $\psi_{m,n}(t)$, the mother wavelet $\psi(t)$ is dilated and translated according to parameters m and n as follows:

$$\psi_{m,n}(t) = 2^{m/2}\psi(2^m t - n). \quad (4)$$

Using Eq. (4) we obtain an orthonormal wavelet basis.¹⁶ Parameter m stretches or compresses the mother wavelet, modifying this function to produce a narrower or broader new function. Therefore all the basis functions $\psi_{m,n}(t)$ have the same profile, that is, the mother wavelet profile, but dilated and translated according to parameters m and n , respectively.

The inverse discrete wavelet transform is given by the reconstruction formula

$$\mathbf{f}(t) = \sum_m \sum_n W_{m,n}(\mathbf{f})\psi_{m,n}(t). \quad (5)$$

In summary, the wavelet transform describes at each resolution step the difference signal between the previous and the current resolution representation. By iterating the process from the highest to the lowest available resolution level, we obtain a pyramidal representation of the signal. The advantage of the wavelet transform defined above is that it relies on an orthogonal transform, so the information difference from one resolution level to the next is nonredundant.

B. À Trous Algorithm

In the discrete case the algorithm described above is not shift invariant, which can be a problem for data fusion. To obtain a shift-invariant discrete wavelet decomposi-

tion for images, we follow Starck and Murtagh,²³ and we use the *à trous* algorithm²⁴ to decompose the image into wavelet planes. Given an image \mathbf{p} we construct the sequence of approximations

$$F_1(\mathbf{p}) = \mathbf{p}_1, \quad F_2(\mathbf{p}_1) = \mathbf{p}_2, \quad F_3(\mathbf{p}_2) = \mathbf{p}_3, \dots$$

To construct the sequence, this algorithm performs successive convolutions with a filter obtained from an auxiliary function called the scaling function. We use a scaling function that has a \mathbf{B}_3 cubic spline profile. The use of a \mathbf{B}_3 cubic spline leads to a convolution with a mask of 5×5 :

$$\frac{1}{256} \begin{bmatrix} 1 & 4 & 6 & 4 & 1 \\ 4 & 16 & 24 & 16 & 4 \\ 6 & 24 & 36 & 24 & 6 \\ 4 & 16 & 24 & 16 & 4 \\ 1 & 4 & 6 & 4 & 1 \end{bmatrix}. \quad (6)$$

As stated above, the wavelet planes are computed as the differences between two consecutive approximations \mathbf{p}_{l-1} and \mathbf{p}_l . Letting $\mathbf{w}_l = \mathbf{p}_{l-1} - \mathbf{p}_l$ ($l = 1, \dots, n$), in which $\mathbf{p}_0 = \mathbf{p}$, we can write the reconstruction formula

$$\mathbf{p} = \sum_{l=1}^n \mathbf{w}_l + \mathbf{p}_r. \quad (7)$$

In this representation the images \mathbf{p}_l ($l = 0, \dots, n$) are versions of the original image \mathbf{p} at increasing scales (decreasing resolution levels), \mathbf{w}_l ($l = 1, \dots, n$) are the multiresolution wavelet planes, and \mathbf{p}_r is a residual image. In our case we use a diadic decomposition scheme. Thus the original image \mathbf{p}_0 has twice the resolution of \mathbf{p}_1 , image \mathbf{p}_1 has twice the resolution of \mathbf{p}_2 , and so on. If the resolution of image \mathbf{p}_0 is, for example, 10 m, the resolution of \mathbf{p}_1 would be 20 m, the resolution of \mathbf{p}_2 would be 40 m, etc. Note, however, that all the consecutive approximations (and wavelet planes) in this process have the same number of pixels as the original image. This is a consequence of the fact that the *à trous* algorithm is an oversampled transform.¹⁹ This is a restriction on the use of this particular wavelet approach for applications such as image compression.

It is interesting to note that the *à trous* algorithm is in some ways similar to the Laplacian pyramid method developed by Burt and Adelson²⁵ to compress images. The Laplacian pyramid method also computes a series of images of decreasing resolution by filtering the original image and the successive approximations with a low-pass filter. The 5×5 mask [relation (6)] used in the *à trous* algorithm is one of the low-pass filters that can be used to construct the Laplacian pyramid. However, in the Laplacian pyramid, once the original image is convolved with the low-pass filter, the resulting image is reduced in size by taking one pixel of each four. Thus the number of pixels decreases by a factor of 4 at each scale. To compute the difference signal (equivalent to the wavelet planes of the *à trous* algorithm), the Laplacian pyramid method expands the decimated image to the size of the image of the previous scale by a Gaussian interpolation with the same low-pass filter.

The Laplacian pyramid method has the advantage that it is easier to understand than the more cumbersome wavelet theory on which the *à trous* algorithm is based. However, the disadvantage of the Laplacian pyramid method is the lack of invariance to translation, which can be a problem in signal analysis, pattern recognition, or, as in our case, data fusion.¹⁹

4. WAVELET IMAGE FUSION METHOD

The wavelet merger method is based on the fact that, in the wavelet decomposition, the images \mathbf{p}_l ($l = 0, \dots, n$) are successive versions of the original image at increasing scales. Thus the first wavelet planes of the high-resolution panchromatic image have spatial information that is not present in the multispectral image. The wavelet-based image merging can be carried out in two ways, as follows.

A. Substitution Method

In the wavelet substitution method some of the wavelet planes of the multispectral image are substituted with planes that correspond to the panchromatic image as follows:

1. Register the low-resolution multispectral image to the same size as the high-resolution panchromatic image so that it is superimposed.

2. As in Section 2, perform histogram matching between the panchromatic image and the intensity component of the color image. Let \mathbf{PAN} be the panchromatic image and \mathbf{R} , \mathbf{G} , and \mathbf{B} be the three bands of the multispectral image.

3. Decompose the R, G, and B bands of the multispectral image to n wavelet planes (resolution levels). Usually, $n = 2$ or 3 . Thus

$$\mathbf{R} = \sum_{l=1}^n \mathbf{w}_{Rl} + \mathbf{R}_r, \quad \mathbf{G} = \sum_{l=1}^n \mathbf{w}_{Gl} + \mathbf{G}_r,$$

$$\mathbf{B} = \sum_{l=1}^n \mathbf{w}_{Bl} + \mathbf{B}_r.$$

4. Decompose the panchromatic high-resolution image accordingly:

$$\mathbf{PAN} = \sum_{l=1}^n \mathbf{w}_{Pl} + \mathbf{PAN}_r.$$

5. Replace the first wavelet planes of the R, G, and B decompositions with the equivalent planes of the panchromatic decomposition.

6. Perform the inverse wavelet transform

$$\mathbf{R}_{\text{new}} = \sum_{l=1}^n \mathbf{w}_{Pl} + \mathbf{R}_r, \quad \mathbf{G}_{\text{new}} = \sum_{l=1}^n \mathbf{w}_{Pl} + \mathbf{G}_r,$$

$$\mathbf{B}_{\text{new}} = \sum_{l=1}^n \mathbf{w}_{Pl} + \mathbf{B}_r.$$

B. Additive Method

Another possibility is to add the wavelet planes of the high-resolution image directly to the multispectral image. The steps of this additive method are the following:

1. Adding to the Red–Green–Blue Components

The first possibility⁸ is to add the high-resolution information directly to the R, G, and B bands. The steps of the method are

1. Register the low-resolution multispectral image and perform histogram matching between the panchromatic image and the intensity component of the color image as above.

2. Decompose only the panchromatic high-resolution image to n wavelet planes (resolution levels). Usually, $n = 2$ or 3 . Thus

$$\mathbf{PAN} = \sum_{l=1}^n \mathbf{w}_{Pl} + \mathbf{PAN}_r.$$

3. Add the wavelet planes of the panchromatic decomposition to the R, G, and B bands of the multispectral image:

$$\mathbf{R}_{\text{new}} = \sum_{l=1}^n \mathbf{w}_{Pl} + \mathbf{R}, \quad \mathbf{G}_{\text{new}} = \sum_{l=1}^n \mathbf{w}_{Pl} + \mathbf{G},$$

$$\mathbf{B}_{\text{new}} = \sum_{l=1}^n \mathbf{w}_{Pl} + \mathbf{B}.$$

2. Adding to the L Component

Another possibility, which we consider to be the best approach, is to incorporate the high-resolution information directly into the intensity component of the multispectral image. As explained in Section 2, we use $L = (R + G + B)/3$ to represent the intensity component. We call this the additive wavelet on L (AWL) method for image merging. Núñez *et al.*²⁶ carried out a preliminary study of this approach. The steps of the method are the following:

Assume steps 1. and 2. as above. Thus

$$\mathbf{PAN} = \sum_{l=1}^n \mathbf{w}_{Pl} + \mathbf{PAN}_r.$$

3. Transform the RGB components of the multispectral image to the LHS representation. Let \mathbf{L} , \mathbf{H} , and \mathbf{S} be the three components of the multispectral image.

4. Add the wavelet planes of the panchromatic decomposition to the \mathbf{L} component as follows:

$$\mathbf{L}_{\text{new}} = \sum_{l=1}^n \mathbf{w}_{Pl} + \mathbf{L}.$$

5. Transform the new LHS values back into the RGB representation.

In the substitution method, the wavelet planes that correspond to the multispectral image are discarded and substituted with the corresponding planes of the panchromatic image. However, in the additive method all the spatial information in the multispectral image is pre-

served. Thus the main advantage of the additive method is that the detail information from both sensors is used. In practice the results of the substitution method are similar to the results of the additive method but slightly defocused, showing that spatial information present only in the multispectral image is lost during the substitution process. Also, the results of the substitution method show some mixed colors in the boundaries of monochromatic areas. Thus here we always prefer the additive method over the substitution method for the fusion of images.

The main difference between adding the panchromatic wavelet planes to the R, G, and B bands as opposed to the L component is that, in the first case, panchromatic information is added in the same amount to all three bands, biasing the color of the pixel toward the gray, whereas in the second case the high-resolution information modifies only the intensity (L), preserving multispectral information in a better way. Thus, from the theoretical point of view, adding to the L component is a better choice than adding to the R, G, and B bands. As stated in Section 2, the reason for using the L component to represent the intensity instead of using I or L' is that I ignores two of the RGB values and, with L' , the increments of intensity (obtained by adding the wavelet planes) are, in some cases, not distributed proportionally to the RGB values.

The advantages of using the wavelet image merging technique over the standard IHS or LHS methods are

1. The spectral quality of the color image is preserved to a high degree.
2. The resolution of the panchromatic image is added to the solution without discarding the resolution of the multispectral image. Thus the detail information from both images is used.
3. The total flux content (mean value) of a wavelet plane is 0. Thus the total flux of the multispectral image is preserved.
4. The AWL method can be considered to be an improvement on the classical IHS/LHS method in the sense that the intensity component is not substituted with the panchromatic image, but the highest resolution features not present in the multispectral image are introduced into the merged image by adding the first wavelet planes of the panchromatic image to the intensity component.

The number (n) of wavelet planes that must be added (or substituted in the substitution method) depends on the ratio between the resolutions of the panchromatic and multispectral images. For example, if the panchromatic image is a 10-m SPOT image and the multispectral image is a 30-m Landsat image, the first wavelet plane of the panchromatic image (w_1) contains the detail information between 10 and 20 m, whereas the second wavelet plane (w_2) contains the spatial information between 20 and 40 m that is greater than the pixel size of the Landsat image. Thus in this case $n = 2$ would suffice. However, in practice the SPOT and Landsat images are taken at different epochs, and for incorporating all the spatial information present in the SPOT image use of another wavelet plane ($n = 3$) is advised.



Fig. 1. Detail of the SPOT image.

5. RESULTS

We applied the above methodology to merge SPOT-PAN and Landsat (TM) images. The original panchromatic SPOT images have 10-m pixels, whereas the original multispectral Landsat (TM) images have 30-m pixels. The SPOT panchromatic band has a spectral response between 0.45 and 0.80 μm with the peak at 0.65 μm . The Landsat original bands were converted to the (RGB) system with the following transformation: $R = (B_5 + B_7)/2$, $G = (B_3 + B_4)/2$, $B = (B_1 + B_2)/2$. The images were registered, and the SPOT image was corrected photometrically to present a histogram similar to the L component of the Landsat image. This photometric correction was carried out by histogram matching as explained in Section 2. Then we applied the AWL image fusion technique and compared the results with those given by the standard methods.

Figure 1 shows detail of the original SPOT image. Figure 2(a) shows the same area of the Landsat image. The spatial resolution of the SPOT image is clearly better than the Landsat image, as expected from the different pixel size. It is easy to see that the SPOT and Landsat images were taken at different epochs. Note, for example, the aspect of the riverbed, the water ponds (black rounded areas in the SPOT image), or the crop fields, which in the SPOT image are clearly different from their appearance in the Landsat image. Also, there are several structures in the SPOT image that were not present when the Landsat image was taken.

Figure 2(b) shows the result of the fusion of the Landsat and SPOT images by the standard IHS method. The increase in resolution with respect to the original Landsat image is evident. Most of the resolution of the SPOT image was incorporated into the result. However, as stated above, there is spectral degradation and intensity dependence of the resulting color and a strong correlation between the merged image and the panchromatic intensity. This fact can be seen qualitatively in the colors of the crop fields and in the aspect of the city streets and of the river-

bed at the bottom of the image, in comparison with the same areas in Fig. 2(a). Figure 2(c) shows the fusion of the same images with the standard LHS method. Here the colors of the fields in the image have a better match with the corresponding colors of Fig. 2(a), but note, for example, the blue color of the water beside the city (black in the Landsat image) as in other areas. Note, also, the aspect of the riverbed and of the city streets, which are similar to those of the IHS result.

Figure 2(d) shows the result of the fusion by the AWL method. In this example three wavelet planes were added. As in the IHS/LHS solution, most of the resolution of the SPOT image was incorporated into the merged image. However, in this case the spectral characteristics

of the Landsat image are preserved better than in the standard mergers. Note the nearly identical tonalities of Figs. 2(a) and 2(d). In particular, the water beside the city is black as in the Landsat image, the bed of the river has the same appearance as in Fig. 2(a), and the streets of the city are better delineated than in the standard results.

Although in this example we do not have any original image (Landsat at 10-m pixels) for comparison, we can quantify the behavior of the AWL method in comparison with the standard methods by computing the correlation of the IHS, LHS, and AWL solutions with regard to the SPOT and Landsat images. To compute the correlation we use the expression

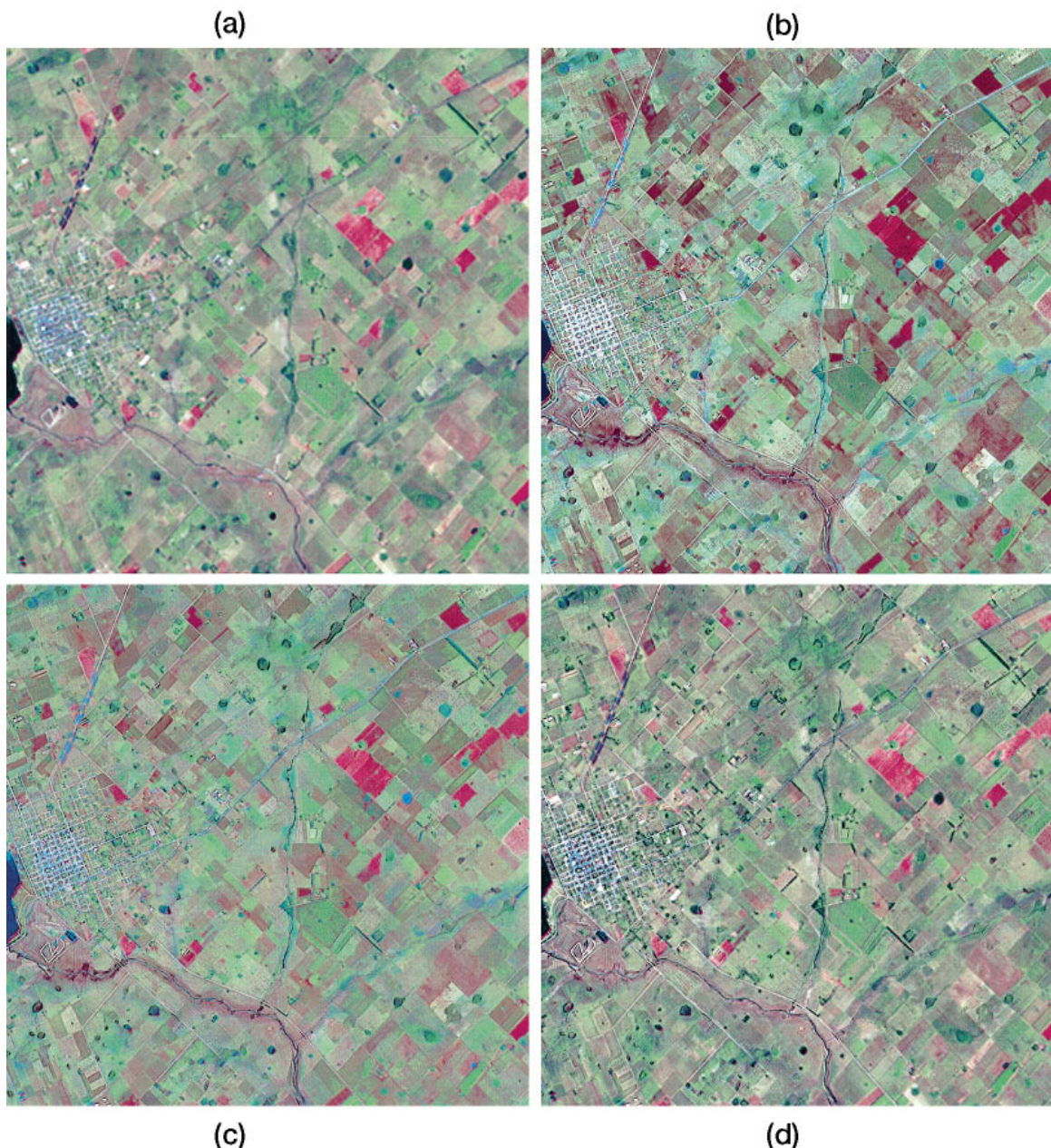


Fig. 2. (a) Detail of the Landsat (TM) image, (b) Result of fusion by the standard IHS method, (c) Result of fusion by the standard LHS method, (d) Result of fusion by the AWL method.

Table 1. Correlation between IHS, LHS, and AWL Merging Methods and SPOT and Landsat (TM) Images

| Images | Correlation | | |
|----------|-------------|-------|-------|
| | Red | Green | Blue |
| TM/SPOT | 0.733 | 0.857 | 0.799 |
| IHS/SPOT | 0.920 | 0.825 | 0.712 |
| LHS/SPOT | 0.813 | 0.905 | 0.828 |
| AWL/SPOT | 0.742 | 0.884 | 0.817 |
| IHS/TM | 0.798 | 0.802 | 0.793 |
| LHS/TM | 0.867 | 0.863 | 0.845 |
| AWL/TM | 0.919 | 0.915 | 0.910 |

$$\text{Corr}(A/B) = 1 - \frac{\sum_{j=1}^{n \text{ pix}} (A_j - B_j)^2}{\sum_{j=1}^{n \text{ pix}} B_j^2}.$$

Note that the target for the correlation is not 1.0, because we do not have any original Landsat images at 10-m pixels with which we can compare the results of the merging methods. Also, a higher correlation with SPOT does not mean a better result.

Table 1 shows the correlations between the solutions with the IHS, LHS, and AWL merging methods and the original Landsat and SPOT images. The first line of Table 1 shows the correlation between the R, G, and B bands of the Landsat (TM) image and the SPOT image. The second and third lines show the correlation between the R, G, and B bands of the IHS and LHS solutions and the SPOT image. The fourth line shows the correlations of the AWL solution. Note that the correlations of the IHS and LHS solutions are higher (especially in R) than the correlations of the AWL solution. This means that the standard solutions are closer to the SPOT image than the AWL solution. However, this is not a weakness of the AWL method. As stated above, there is a strong correlation between the IHS and LHS merged images and the intensity of the panchromatic image. This excessively high correlation produces solutions that are closer than desirable to the SPOT image. The correlation is however, lower in the additive wavelets solution. This is a positive result, because it indicates a lower dependence of the AWL solution on the SPOT image.

Lines 5–7 in Table 1 indicate the correlation between the same solutions as above and the Landsat (TM) image. Note that the correlation of our AWL solution is higher than of the IHS and LHS merging methods. This means that, as stated above in qualitative terms, the additive wavelet solution on L preserves the spectral characteristics of the multispectral image to a greater extent than the IHS and LHS solutions. Thus the additive wavelet solution on L behaves better than the standard methods.

6. CONCLUSIONS

The AWL method combines a high-resolution panchromatic image and a low-resolution multispectral image by

the addition of some wavelet planes of the panchromatic image to the intensity component [defined as $L = (R + G + B)/3$] of the low-resolution image. With this method, the detail information from both images is preserved. The method is capable of enhancing the spatial quality of the multispectral image while preserving its spectral content to a greater extent. The AWL method does not modify the total flux of the multispectral image, since the mean value of each of the added wavelet planes is 0. The AWL method can be considered to be an improvement on the classical IHS or LHS methods in the sense that the intensity is not substituted by the panchromatic image but the high-resolution of the panchromatic image is injected into the merged image by the addition of some wavelet planes of the panchromatic image to the intensity component of the multispectral low-resolution image.

ACKNOWLEDGMENTS

This work was supported in part by the Dirección General de Investigación Científica y Técnica Ministerio de Educación y Ciencia (Spain) under grants BP95-1031-A and PB97-0903. Partial support was also obtained from the Institut Cartogràfic de Catalunya, the Direcció General d'Universitats Generalitat de Catalunya, and from the Gaspar de Portolà Catalan Studies Program of the University of California.

J. Núñez's e-mail address is jorge@fajnm1.am.ub.es.

REFERENCES

1. T. Taxt and A. H. Schistad-Solberg, "Data fusion in remote sensing," in *Proceedings of the Fifth International Workshop on Data Analysis in Astronomy*, V. Di Gesu and L. Scarsi, eds. (World Scientific, Singapore, 1996), pp. 269–280.
2. P. S. Chavez, S. C. Sides, and J. A. Anderson, "Comparison of three different methods to merge multi-resolution and multispectral data: Landsat TM and SPOT panchromatic," *Photogramm. Eng. Remote Sens.* **57**, 295–303 (1991).
3. J. C. Tilton, ed., *Proceedings of Conference on Multisource Data Integration in Remote Sensing*, NASA Conf. Publ. 3099 (NASA, Washington, D.C., 1991).
4. J. W. Carper, T. M. Lillesand, and R. W. Kiefer, "The use of intensity-hue-saturation transformations for merging SPOT panchromatic and multispectral image data," *Photogramm. Eng. Remote Sens.* **56**, 459–467 (1990).
5. V. K. Shettigara, "A generalized component substitution technique for spatial enhancement of multispectral images using a higher resolution data set," *Photogramm. Eng. Remote Sens.* **58**, 561–567 (1992).
6. M. Datcu, D. Luca, and K. Seidel, "Multiresolution analysis of SAR images," in *Proceedings of the European Conference on Synthetic Aperture Radar (VDE-Verlag GmbH, Berlin, 1996)*, pp. 375–378.
7. D. A. Yocky, "Image merging and data fusion by means of the discrete two-dimensional wavelet transform," *J. Opt. Soc. Am. A* **12**, 1834–1841 (1995).
8. D. A. Yocky, "Multiresolution wavelet decomposition image merger of LANDSAT thematic mapper and SPOT panchromatic data," *Photogramm. Eng. Remote Sens.* **62**, 1067–1074 (1996).
9. B. Garguet-Duport, J. Girel, J. M. Chassery, and G. Pautou, "The use of multiresolution analysis and wavelets transform for merging SPOT panchromatic and multispectral

- image data," *Photogramm. Eng. Remote Sens.* **62**, 1057–1066 (1996).
10. T. Ranchin, L. Wald, and M. Mangolini, "The ARSIS method: a general solution for improving spatial resolution of images by the means of sensor fusion," in *Proceedings of the Conference on Fusion of Earth Data*, T. Ranchin and L. Wald, eds. (SEE/URISCA, Nice, France, 1996), pp. 53–58.
 11. J. Núñez, X. Otazu, O. Fors, and A. Prades, "Simultaneous image fusion and reconstruction using wavelets. Applications to SPOT+LANDSAT images," *Vistas Astron.* **41**, 351–357 (1997).
 12. A. R. Smith, "Color gamut transform pairs," *Comput. Graph.* **12**, 12–19 (1978).
 13. Association for Computing Machinery, "Status report of the graphics Standard Planning Committee," *Comput. Graph.* **13**, (1979).
 14. Y. Meyer, *Wavelets. Algorithms and Applications* (SIAM Press, Philadelphia, Pa., 1993).
 15. R. K. Young, *Wavelet Theory and its Applications* (Kluwer Academic, Boston, 1993).
 16. I. Daubechies, *Ten Lectures on Wavelets* (SIAM Press, Philadelphia, Pa., 1992).
 17. C. K. Chui, *An Introduction to Wavelets* (Boston Academic, Boston, 1992).
 18. G. Kaiser, *A Friendly Guide to Wavelets* (Birkhauser, Boston, 1994).
 19. M. Vetterli and J. Kovacevic, *Wavelets and Subband Coding* (Prentice Hall, Englewood Cliffs, N.J., 1995).
 20. J. L. Starck and E. Pantin, "Multiscale maximum entropy image restoration," *Vistas Astron.* **40**, 563–569 (1996).
 21. F. Rué and A. Bijaoui, "A multiscale vision model applied to astronomical images," *Vistas Astron.* **40**, 495–502 (1996).
 22. S. Mallat, "A theory for multiresolution signal: the wavelet representation," *IEEE Trans. Pattern. Anal. Mach. Intell.* **11**, 674–693 (1989).
 23. J. L. Starck and F. Murtagh, "Image restoration with noise suppression using the wavelet transform," *Astron. Astrophys.* **288**, 342–350 (1994).
 24. M. Holschneider and P. Tchamitchian, "Regularité local de la fonction 'non-differentiable' de Riemann," in *Les ondelettes in 1989*, P. G. Lemarié, ed., *Lecture Notes in Mathematics* No. 1438 (Springer-Verlag, Berlin, 1990), pp. 102–124.
 25. P. J. Burt and E. H. Adelson, "The Laplacian pyramid as a compact image code," *IEEE Trans. Commun.* **COM-31**, 532–540 (1983).
 26. J. Núñez, X. Otazu, O. Fors, and A. Prades, "Fusion and reconstruction of LANDSAT and SPOT images using wavelets," in *Proceedings of the Second Conference on Fusion of Earth Data*, T. Ranchin and L. Wald, eds. (SEE/URISCA, Nice, France, 1998), pp. 103–108.